MULTIPARAMETRIC SMOOTHING BASED ON MEAN SHIFT PROCEDURE FOR ULTRASOUND DATA SEGMENTATION

Thomas Grenier, Chantal Revol-Muller, Franck Davignon, Olivier Basset, Gérard Gimenez

CREATIS, CNRS UMR 5515, Inserm U 630, Bât. B. Pascal, 69621 Villeurbanne, France
phone : + (33) 472 43 81 91, fax: + (33) 472 43 85 26, email: chantal.muller@creatis.insa-lyon.fr
web: www.creatis.insa-lyon.fr

ABSTRACT

Segmentation of ultrasound data is improved when using multi-parametric approach. In this paper we propose the use of Multi-Parametric Mean Shift procedure (MPMS). Two derived processes are described: MPMS smoothing which achieves a multi-parametric filtering in the spatial-range domain and MPMS segmentation which takes benefit of this filtering for segmenting the multidimensional data. MPMS segmentation is particularly attractive, since it achieves an unsupervised segmentation. These methods were positively tested on three sets of simulated ultrasonic data, representative of various scatterers densities and also various scattering conditions.

1. INTRODUCTION

Several approaches have been proposed for the segmentation of ultrasonic images. Most of them are based on the pixel intensity and use either an active contour or a Bayesian framework in order to define an energy function that characterizes a homogeneous region or a contour. The poor quality of conventional ultrasonic images and the slight differences between the various tissues make the automatic segmentation difficult.

Among the region-based approaches described in the literature, Ashton and Parker [1] have proposed a modification of an adaptive clustering algorithm for taking into account the particularities of ultrasonic data. Spatial smoothness constraints are incorporated in the algorithm by the use of a Markov Random Field (MRF) which models the region process. Implementation of these algorithms involves a priori information about the intensity distribution of the various tissues [2].

An intensity-amplitude invariant approach using a phased-based feature detection method has been proposed in [3]. Applied to an echocardiographic image sequence, the algorithm takes advantage of the temporal inconsistency of speckle for detecting the acoustic boundaries. In [4], a linear combination of the pixel grey level and of the local entropy is used in the "Minimum Cross Entropy Thresholding" technique for segmenting ultrasonic images. This original method can be generalized to a multivariate thresholding based on several image parameters.

In this study, we propose a method for segmenting ultrasound data from a set of parametric images. These parametric images derive from tissue characterisation techniques and are calculated on envelope echographic images or on Radio Frequency (RF) signals. At first, a multidimensional filtering based on the mean shift technique is performed in the joint spatial-range domain [5]. This technique consists in assigning each pixel with a local mode of the underlying distribution. The local modes are identified by an iteratively moving kernel in both spatial and range domains. The final segmentation is obtained from the resulting multidimensional filtered image, by fusing regions associated with nearby modes.

2. ULTRASOUND AND PARAMETRIC IMAGES

The conventional image used by the radiologist during an ultrasonic examination is the B-mode image computed from the envelope of the RF signal. In the B-mode, only a reduced part of the whole information given by the original signal is exploited. However, some additional acoustical parameters representative of the scatterers properties within the tissues can be extracted from the RF signal. Those parameters can provide two kinds of information: the echogenicity properties of the scatterers and the spatial organisation of the scatterers. In our application, the envelope intensity of the RF signal and two parameters related to the spatial organisation of the scatterers will be considered. The first parameter $\hat{\alpha}_2$ estimates the scatterers density, the second one called Ω gives some information about the scattering conditions and derives from the Nakagami distribution. The proposed method will be tested on ultrasonic data simulated with the Field software [6]. Given the positions and the acoustical characteristics of the scatterers, as well as the beam characteristics, this software is able to compute the emitted and received waves, thus creating the corresponding RF signals.

2.1 Scatterers density estimator $\hat{\alpha}_2$

The literature shows that the spatial organisation of the scatterers can be evaluated from the 2D envelope image [7]. It has been shown that according to the density range and spatial organisation of the scatterers, the intensity of the envelope can be modelled by several distributions [8].

The spatial organisation of the scatterers in the tissue can be estimated by computing a density estimator. In the case of a medium without regularly spaced scatterers, the resulting echo is a coherent sum of reflected waves from randomly distributed scatterers. If the number of scatterers per

resolution cell is greater than 10, the amplitude of the envelope signal is Rayleigh distributed. For smaller densities, the envelope is modelled with a K-distribution. Its density probability function is given in eq. (1) :

$$p(A) = \frac{2b}{\Gamma(\alpha)}\left(\frac{b.A}{2}\right)^{\alpha} K_{\alpha-1}(b.A) \quad (1)$$

where :

$b = 2\sqrt{\frac{\alpha}{E[A^2]}}$ and Γ is defined so that $\begin{cases}\Gamma(u+1) = u.\Gamma(u)\\ \Gamma(1) = 1\end{cases}$ (2)

with $E[]$ the statistical average, A the envelope signal, K_n the modified second Bessel function of order n and α the effective number of scatterers per resolution cell.

Ossant et al. have proposed an estimator of α, called $\hat{\alpha}_2$, based on low order moments [9]. Its computation is given by eq. (3):

$$\frac{\Gamma(\alpha+1).\Gamma(\alpha)}{\Gamma^2(\alpha+1/2)} = \frac{E[A^2]}{E^2[A]}.\frac{\Gamma(3/2)}{\Gamma(2)} \quad (3)$$

The right part of eq. (3) can be computed from the envelope image. To determine the estimate $\hat{\alpha}_2$ of α, equation (3) is numerically solved using a dichotomy algorithm.

2.2 Nakagami distribution

According to the scatterers density, the Nakagami distribution [10] covers the whole range of envelope statistics: Rayleigh, pre-Rayleigh (K-distribution) and post-Rayleigh (Rice). The probability density function (pdf) is expressed as follows:

$$f(A) = \frac{2m^m A^{2m-1}}{\Gamma(m)\Omega^m}\exp\left(-\frac{m}{\Omega}A^2\right)U(A) \quad (4)$$

where $U(A)$ is the unit step function. For the Nakagami distribution, Ω is the scaling parameter and m is the shape parameter. m and Ω can be estimated as:

$$m = \frac{\Omega^2}{E[A^2-\Omega]^2} \quad \text{and} \quad \Omega = E[A^2] \quad (5)$$

2.3 Numerical phantoms

Three numerical phantoms were used for the simulation, resulting in three sets of ultrasonic data. They mimic lesions in the structure of the tissue. The first phantom is a low-density and lowly scattering lesion (*data 1*), the second one consists in a high-density and highly scattering lesion (*data 2*), and the third one shows a high-density lesion (*data 3*). The geometry of the two-region phantoms is shown in Fig. 1.

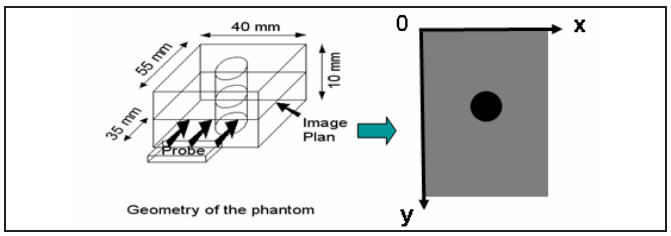

Figure 1: Geometry of the phantom

3. MULTIDIMENSIONAL MEAN SHIFT

Mean shift is a non parametric estimator of density gradient developed by Fukunaga and Hostetler thirty years ago [11] and recently exploited in low level computer vision tasks by Comaniciu and Meer ([12],[5]). Mean shift framework is interesting because it jointly takes into account both spatial information (pixel location in the spatial domain R^s) and range information (gray level, color or spectral information in the range domain R^r). The resulting spatial-range domain is represented by a d-dimensional Euclidian space R^d, where $d = s + r$. Moreover, the mean shift technique is also attractive, since it doesn't need prior knowledge about pixel intensity distribution. In this paper, we propose a multidimensional range implementation of the **M**ean **S**hift that takes into account the **M**ulti-**P**arametric images computed from the envelope of the RF ultrasonic signal. We called this algorithm (MPMS).

3.1 Principle of mean shift procedure

The mean shift procedure was fully described in [5]. In this section, we remind the general principle and the main equations governing the method.

The mean shift method is based on the kernel density estimation. In eq. 6, the multivariate kernel density estimator with kernel K (a radially symmetric, non-negative function centred at zero and integrating to one) and a symmetric, positive definite bandwidth matrix **H** is defined for a set of n data points $\{\mathbf{x}_i\}_{i=1,\ldots n}$ in a d-dimensional Euclidian space R^d. In this expression, the density at each point **x** is estimated using the same scaled kernel over the whole data points.

$$\hat{f}(\mathbf{x}) = \frac{1}{n}\sum_{i=1}^{n} K_{\mathbf{H}}(\mathbf{x}-\mathbf{x}_i) \quad (6)$$

The bandwidth **H** scales the kernel support to be radial symmetric.

$$K_{\mathbf{H}}(\mathbf{u}) = (\det[\mathbf{H}])^{-\frac{1}{2}} K\left(\mathbf{H}^{-\frac{1}{2}}\mathbf{u}\right) \quad (7)$$

In our application, we will restrict **H** to a diagonal matrix. Each element h_n (n = 1,…, d) of the matrix is the scale parameter of the n^{th} dimension of the d-dimensional Euclidian space R^d.

$$\mathbf{H} = \begin{bmatrix} h_1 & 0 & 0 \\ 0 & \ddots & 0 \\ 0 & 0 & h_d \end{bmatrix} \quad (8)$$

Due to its symmetry property, K(**u**) can be replaced by its profile $k : [0,\infty) \to R$, a monotonically decreasing function:

$$K(\mathbf{u}) = c_{k,d}.k(\mathbf{u}^T\mathbf{u}) \quad with \begin{cases} k(u) \geq 0 \ for \ 0 \leq u \leq 1 \\ k(u) = 0 \ for \ u > 1 \end{cases} \quad (9)$$

where $c_{k,d}$ is a normalization constant.

Eq. 6 can be rewritten taking into account eq. 7 and eq. 9

$$\hat{f}(\mathbf{x}) = \frac{c_{k,d}}{n}(\det[\mathbf{H}])^{-\frac{1}{2}}.\sum_{i=1}^{n} k\left((\mathbf{x}-\mathbf{x}_i)^T\mathbf{H}^{-1}(\mathbf{x}-\mathbf{x}_i)\right) = \frac{c_{k,d}}{n}(\det[\mathbf{H}])^{-\frac{1}{2}}.\sum_{i=1}^{n} k\left(d[\mathbf{x},\mathbf{x}_i,\mathbf{H}]^2\right) \quad (10)$$

where $d[\mathbf{x}, \mathbf{x}_i, \mathbf{H}_i]^2$ denotes the square Mahalanobis distance from **x** to $\mathbf{x}_i$.

Using the linearity property of eq. 10, the density gradient estimator is obtained as the gradient of the density estimator in eq. 11.

$$\hat{\nabla} f(\mathbf{x}) \equiv \nabla \hat{f}(\mathbf{x}) = \frac{2c_{k,d}}{n}.\left(\det[\mathbf{H}]\right)^{-\frac{1}{2}}.\sum_{i=1}^{n}\mathbf{H}^{-1}.(\mathbf{x}-\mathbf{x}_i).k'\left(d[\mathbf{x},\mathbf{x}_i,\mathbf{H}]^2\right) \quad (11)$$

This expression can be rewritten with $g(u) = -k'(u)$.

$$\hat{\nabla} f(\mathbf{x}) = \frac{2c_{k,d}\mathbf{H}^{-1}}{n.\left(\det[\mathbf{H}]\right)^{\frac{1}{2}}}.\left(\sum_{i=1}^{n} g\left(d[\mathbf{x},\mathbf{x}_i,\mathbf{H}]^2\right)\right)\times \left[\left(\sum_{i=1}^{n} g\left(d[\mathbf{x},\mathbf{x}_i,\mathbf{H}]^2\right)\right)^{-1}.\sum_{i=1}^{n} g\left(d[\mathbf{x},\mathbf{x}_i,\mathbf{H}]^2\right)\mathbf{x}_i - \mathbf{x}\right] \quad (12)$$

The mean shift vector is defined in eq. 13. It was shown that this vector is an estimator of the normalized gradient of the underlying distribution.

$$M(\mathbf{x}) = \left(\sum_{i=1}^{n} g\left(d[\mathbf{x},\mathbf{x}_i,\mathbf{H}]^2\right)\right)^{-1}.\sum_{i=1}^{n}\mathbf{x}_i\, g\left(d[\mathbf{x},\mathbf{x}_i,\mathbf{H}]^2\right) - \mathbf{x} \quad (13)$$

The main property of this estimator is the convergence associated with its repetitive computation. The mean shift procedure consists in an iterative computation of the mean shift vector $M(\mathbf{x})$ and the translation of the kernel by $M(\mathbf{x})$. It was proved that this process converges at a point where the estimate has zero gradient i.e. $\|M(\mathbf{x})\| \approx 0$.

Starting from a point $\mathbf{x} = \mathbf{x}^{[1]}$, the successive locations of the kernel are stored by the sequence $\{x^{[l]}\}_{l=1,2,..}$ given by eq. 14.

$$\mathbf{x}^{[l+1]} = \left(\sum_{i=1}^{n} g\left(d[\mathbf{x}^{[l]},\mathbf{x}_i,\mathbf{H}]^2\right)\right)^{-1}.\left(\sum_{i=1}^{n}\mathbf{x}_i.g\left(d[\mathbf{x}^{[l]},\mathbf{x}_i,\mathbf{H}]^2\right)\right) \quad (14)$$

At each iteration, $\left\|M(\mathbf{x})^{[l+1]}\right\| = \left\|\mathbf{x}^{[l+1]} - \mathbf{x}^{[l]}\right\|$ is evaluated. The process stops when the module of the mean shift vector is less than a tolerance threshold. The point of convergence $\mathbf{x}_{conv}$ corresponds to the mode of the distribution.

3.2 MPMS smoothing

In our application, ultrasonic data include three bi-dimensional parametric images: the ultrasonic envelope image, an image of the local scatterers density estimation and an image of the feature Ω estimated from the Nakagami distribution (see Section 2). So, each point $\mathbf{x}_i$ is described by 5 coordinates x_i^j (j=1, …5): x_i^1 and x_i^2 represent the spatial location and the last three ones indicate the grey levels of the parametric data. MPMS smoothing takes into account those 5 dimensions.

The image filtering consists in applying the mean shift procedure to each pixel $\{\mathbf{x}_i\}_{i=1,...n}$ of the original image and by assigning to each pixel $\{\mathbf{y}_i\}_{i=1,...n}$ of the filtered image the components of the point of convergence $\mathbf{x}_{conv}$ associated to $\mathbf{x}_i$.

The features required by MPMS are the diagonal entries of the matrix $\mathbf{H}$. h^1 and h^2 denote the spatial scale parameters and h^3, h^4 and h^5 denote the range scale parameters. Those scale parameters control the size of the kernels used for detecting the modes of the underlying multidimensional density. As we use two spherical kernels for the spatial domain ($h^1 = h^2 = h_s$) and also for the range domain ($h^3 = h^4 = h^5 = h_r$), only both parameters h_s and h_r are needed.

3.3 MPMS segmentation

The final segmentation is obtained from the resulting multidimensional filtered image, by fusion of the regions associated with nearby modes. Clusters are identified by linking together all filtered pixels which are closer than a normalised distance in the spatial-range domain. In order to clearly distinguish the different clusters and consequently improve the resulting segmentation, MPMS filtering can be iterated several times before this fusion step.

4. RESULTS AND DISCUSSION

We have tested MPMS smoothing on the three sets of multi-dimensional ultrasonic data previously defined in Section 2 with (h_s, h_r) = (10, 70). In order to evaluate the results, the reference image used for the simulation is given in Fig.3a. In Fig.2, the filtering effect of MPMS can be observed separately on each range component of *data 1,* in order to see the contribution of each parametric image. Each of the three range components has been well smoothed. MPMS has reduced the speckle noise while preserving a high quality discontinuity.

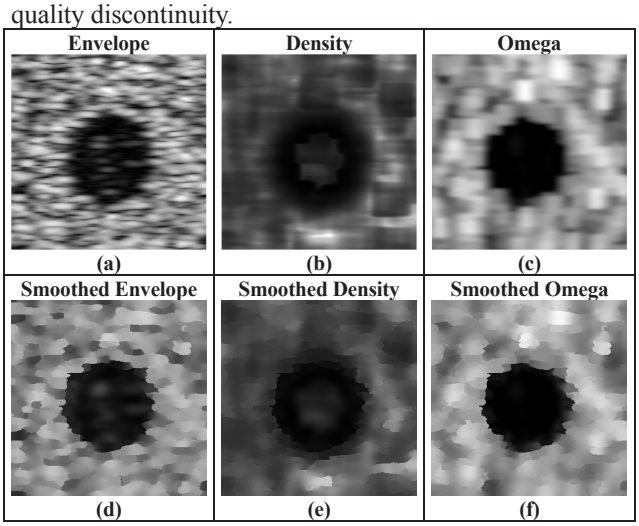

Figure 2: Range components a), b) ,c) of *data 1* and smoothing effect d), e), f) by MPMS (h_s=10, h_r= 70).

For clarity purpose, the multi-parametric information was synthesised in only one image called "fuzzed image". This image displays for each pixel the value of a special norm computed from the range components of the multi-dimensional data. The grey levels of the fuzzed image are computed using eq.15:

$$greylevel_i = \sqrt{\left(x_i^3\right)^2 + \left(x_i^4\right)^2 + \left(x_i^5\right)^2} \quad (15)$$

In Fig. 3, we compare visually a fuzzed image obtained directly from *data 1* and a fuzzed image obtained after MPMS smoothing applied to the same data. The image in Fig. 3c appears more homogeneous and the dark blob shape is also closer to the ideal one (Fig. 3a). Hence, the shape under-estimation of the obtained structure using ultrasound is slightly corrected by MPMS smoothing effect.

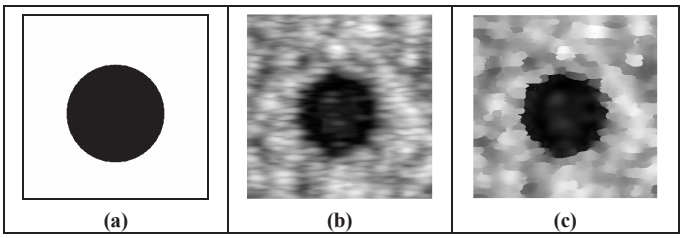

Figure 3: a) the phantom reference image and fuzzed images b) before and c) after filtering by MPMS obtained with *data 1*.

We choose to illustrate the impact of MPMS smoothing on segmentation results. For both the original data and filtered data, the fuzzed image and every range component were segmented using the Otsu automated thresholding [13]. To measure the thresholding accuracy, classical correct detection rates (*cdr*) were computed. Corresponding results, in percentage, are given in Fig. 4. For all tested data, Fig. 4 shows that after MPMS filtering, the number of misclassified pixels has decreased by 24% in average.

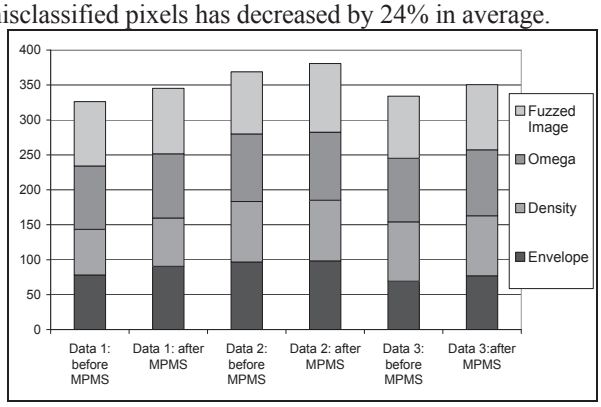

Figure 4: Parameters *cdr* related to the Otsu thresholding computed from the fuzzed images and every range component, before and after MPMS smoothing.

The MPMS segmentation has been computed from the resulting filtered data. In the present case, in order to increase the filtering effect, we iterated MPMS smoothing 10 times before starting the segmentation process. In Fig. 5, the results of MPMS segmentation obtained from the three sets of ultrasonic data are illustrated. MPMS segmentation discriminates correctly the dark blob from the background without specifying the number of clusters. The values of the *cdr* parameters are all higher than 94 %, confirming the efficiency of our method and its superiority over the automated thresholding.

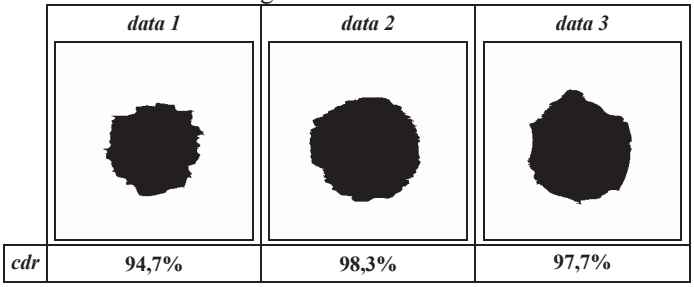

Figure 5: Results of MPMS segmentation from the three sets of ultrasonic data and evaluation of the segmentation accuracy.

5. CONCLUSION

A mean shift based multi-parametric algorithm (MPMS) has been successfully tested to improve simulated ultrasound images segmentation. In our application, the multi-dimensional aspect consists in combining three images (envelope, density and a parameter of the Nakagami distribution). Two derived processes are described: MPMS smoothing which achieves a multi-parametric filtering and MPMS segmentation which takes benefit of the filtering for segmenting data. We have proved the efficiency of MPMS smoothing by evaluating the quality of an automated thresholding after the filtering step. Similarly, MPMS segmentation taking into account the 5 filtered components in the joint domain outperforms the automated thresholding.

REFERENCES

[1] E. A. Ashton and K. J. Parker, "Multiple resolution bayesian segmentation of ultrasound imaging," *Ultrasonic Imaging*, vol. 17, pp. 291-304, 1995.

[2] D. Boukerroui, O. Basset, A. Noble, and A. Baskurt, "Segmentation of ultrasound images - Multiresolution 2D and 3D algorithm based on global and local statistics," *Pattern Recognition Letters*, vol. 24, pp. 779-790, 2003.

[3] M. Mulet-Parada and J. A. Noble, "2D+T Boundary Detection in Echocardiography," *Med. Image Anal.*, vol. 4, pp. 21-30, 2000.

[4] Y. Zimmer, R. Tepper, and S. Akselrod, "A Two-dimensional Extension of Minimum Cross Entropy Thresholding for the Segmentation of Ultrasound Images," *Ultrasound in Medicine and Biology*, vol. 22, pp. 1183-1190, 1996.

[5] D. Comaniciu and P. Meer, "Mean shift: A robust approach toward feature space analysis," *IEEE Transactions on Pattern Analysis and Machine Intelligence*, vol. 24, pp. 603-619, 2002.

[6] J. A. Jensen and P. Munk, "Computer Fantoms for Simulation Ultrasound B-mode and CFL Images," presented at 23rd Acoust. Imag. Symp., Boston, MA, 1997.

[7] J. M. Thijssen, "Ultrasonic Speckle Formation, Analysis and Processing applied to Tissue Characterization," *Pattern Recognition Letters*, vol. 24, pp. 659-675, 2003.

[8] E. Jakeman and R. J. A. Tough, "Generalized K-distribution : A statistical model for weak scattering," *J. Opt. Soc. Am.*, vol. 4, pp. 1764-1772, 1987.

[9] F. Ossant, F. Patat, M. Lebertre, M.-L. Teriierooiterai, and L. Pourcelot, "Effective Density Estimators based on the K-distribution: Interest of Low and Fractional Order Moments," *Ultrasonic Imaging*, vol. 20, pp. 243-259, 1998.

[10] P. M. Shankar, V. A. Dumane, J. M. Reid, V. Genis, F. Forsberg, C. W. Piccoli, and B. B. Goldberg, "Classification of Ultrasonic B-mode Images of Breast Masses using Nakagami Distribution," *IEEE Transactions on Ultrasonics, Ferroelectrics, and Frequency Control*, vol. 48, pp. 569-580, 2001.

[11] K. Fukunaga and L. D. Hostetler, "Estimation of the gradient of a density function with applications in pattern recognition.," vol. IT-21, pp. 32-40, 1975.

[12] D. Comaniciu and P. Meer, "Mean shift analysis and applications," presented at Proceedings of the 1999 7th IEEE International Conference on Computer Vision (ICCV'99), Sep 20-Sep 27 1999, Kerkyra, Greece, 1999.

[13] M. Sezgin and B. Sankur, "Survey over image thresholding techniques and quantitative performance evaluation," *Journal of Electronic Imaging*, vol. 13, pp. 146-168, 2004.